

EARLY CAREER SCHOLARS IN MATERIALS SCIENCE

Influence of side-chain isomerization on the isothermal crystallization kinetics of poly(3-alkylthiophenes)

Zhiyuan Qian^{1,b)}, Shaochuan Luo^{2,b)}, Tengfei Qu², Luke A. Galuska¹, Song Zhang¹, Zhiqiang Cao¹, Sujata Dhakal¹, Youjun He³, Kunlun Hong^{3,4}, Dongshan Zhou², Xiaodan Gu^{1,a)}

Received: 23 June 2020; accepted: 28 July 2020; published online: 1 February 2021

Flexible alkyl side chain in conjugate polymers (CPs) improves the solubility and promotes solution processability, in addition, it affects interchain packing and charge mobilities. Despite the well-known charge mobility and morphology correlation for these semi-crystalline polymers, there is a lack of fundamental understanding of the impact of side chain on their crystallization kinetics. In the present work, isothermal crystallization of five poly(3-alkylthiophene-2,5-diyl) (P3ATs) with different side-chain structures were systematically investigated. To suppress the extremely fast crystallization and trap the sample into amorphous glass, an advanced fast scanning chip calorimetry technique, which is able to quench the sample with few to tens thousands of K/s, was applied. Results show that the crystallization of P3ATs was greatly inhibited after incorporation of branched side chains, as indicated by a dramatic up to six orders of magnitude decrease in the crystallization rate. The suppressed crystallization of P3ATs were correlated with an increased π - π stacking distance due to unfavorable side-chain steric interaction. This work provides a pathway to use side-chain engineering to control the crystallization behavior for CPs, thus to control device performance.



Xiaodan Gu earned his Ph.D. from the Department of Polymer Science and Engineering at the University of Massachusetts Amherst, advised by Prof. Thomas P. Russell, focusing on the self-assembly of block copolymers and their lithographic applications. Subsequently, he started a post-doctoral appointment co-advised by Zhenan Bao and Michael F. Toney at Stanford University and SLAC National Accelerator Laboratory, where he studied the morphology of roll-to-roll printed electronics using real-time X-ray scattering techniques. He moved to the University of Southern Mississippi to start his independent career in 2016. His current research interests revolve around various fundamental polymer physics phenomena related to conjugated polymers and their derivative devices. His group studies structure, dynamic, and morphology of conjugated polymers and aim to link their molecular structures to their macroscopic properties through advanced metrology with an emphasis on scattering techniques. He was awarded ORAU Powe Junior Faculty Enhancement Award in 2019, ACS PMSE Young investigator, and a contributor to "Young Talents" special issue to Macromolecular Rapid Communications, "Emerging investigator" for 2020 Polymer Chemistry, and " Early Career Scholars" for 2021 Journal of Materials Research from MRS.

¹School of Polymer Science and Engineering, Center for Optoelectronic Materials and Devices, The University of Southern Mississippi, Hattiesburg, Mississippi 39406, USA

²Department of Polymer Science and Engineering, School of Chemistry and Chemical Engineering, Key Laboratory of High Performance Polymer Materials and Technology of Ministry of Education, and The State Key Laboratory of Coordination Chemistry, Nanjing University, Nanjing 210093, P.R. China

³Center for Nanophase Materials Sciences, Oak Ridge National Laboratory, Oak Ridge, Tennessee 37831, USA

⁴Department of Chemical and Biomolecular Engineering, University of Tennessee, Knoxville, Tennessee 37996, USA

a) Address all correspondence to this author. e-mail: xiaodan.gu@usm.edu b) These authors contributed equally.



Introduction

Conjugated polymers (CPs) have attracted significant attention owing to their wide range of applications in electronic devices, including organic photovoltaic cells (OPV), organic lightemitting diode (OLED), organic field-effect transistor (OFET), etc. [1, 2]. Recent advances in device performance demonstrated its great potential for commercialization of next-generation flexible electronics. For example, through chain alignment, charge carrier mobility performance of more than 20 cm²/V s has been reported for donor-acceptor (D-A) CPs [3, 4], which is comparable to the performance of polycrystalline silicon [5]; OPV solar cell consists of CP donors and non-fullerene acceptors (NFAs) has achieved a power conversion efficiency (PCE) over 17% [6], a record high efficiency up to date.

The structure of CPs consists of planar and rigid backbone with delocalized electronic cloud to facilitate charge transport and flexible alkyl side chain to improve solubility. Researches have extensively focused on improving the performance by tuning the chemistry of building blocks to reduce π – π stacking distance and increase overlaps of π -orbitals to promote interchain hopping [5, 7]. For example, it has been found that apart from improving the solubility for solution processability, incorporation of side chain also affects chain packing and subsequently charge mobility [8]. In general, steric hindrance effect increases as alkyl chain length increase or as side chain becomes bulkier, which interrupts chain packing and increases π - π stacking distance as well as lamellar spacing, and then reduces charge mobility [9]. Besides, D-A CPs are often synthesized with bulky branched side chains, by replacing them partially with linear chains, it boosts the charge mobility due to less steric hinderance, better interchain packing, and enhancement in crystallinity [8].

Despite the various donor and acceptor moieties, a general consensus that interconnected ordered microstructure network including crystallites and aggregates can improve charge carrier mobility, has been reached for the high mobility CPs [7, 10]. For instance, polythiophene-based CPs including poly(3-hexylthiophene-2,5-diyl) (P3HT) and poly(2,5-bis(3-tetradecylthiophen-2-yl)thieno[3,2,-b]thiophene) (PBTTT), the charge mobility has been shown to be correlated with degree of crystallinity and ordered crystalline domain size [11]. Although post-treatments such as thermal annealing and solvent annealing have been widely used to improve crystallinity of CPs, fundamental crystallization phenomena have been largely overlooked with the exceptions on the model CPs systempoly(3-alkylthiophenes) (P3AT). Studies have been carried on the P3ATs with linear alkyl side chain, for example, poly (3-butylthiophene) (P3BT) [12], P3HT [13, 14, 15], poly (3-octylthiophene) (P3OT) [12, 13], and poly(3-dodecylthiophene) (P3DDT) [12, 13], and obtained equilibrium melting temperature (T_m^0) and enthalpy of fusion of ideal crystals (ΔH_u^0) . In addition, numerous other factors that govern the crystallization behaviors have been reported, including regioregularity [16], molecular weight [10], nucleation density [17], etc. For instance, Treat et al. have utilized a commercially available nucleating agent to facilitate the crystallization of P3HT by increasing its crystallization temperature, without affecting charge mobility [17].

Besides P3ATs with linear side chains, Segalman and co-workers have extended their research interests to branched side-chain poly(3-(2'-ethyl)hexyl-thiophene) (P3EHT) and obtained a melting temperature (Tm) of approximately 80 °C [18]. This is a significant decrease in $T_{\rm m}$, as high as 100 °C, compared to its linear counterpart P3OT, which possesses a $T_{\rm m}$ of approximately 170 °C [13]. In addition, P3EHT exhibits a slow crystallization kinetics, the crystallization completes after several hours of isothermal annealing, which enables real-time investigation to correlate the crystallinity with optoelectronic performance [19, 20]. Hence, its isothermal crystallization kinetics after quenching to supercooled state can be investigated with X-ray [19, 20] and conventional differential scanning calorimetry (DSC) [21], and analyzed with Avrami equation [22], which has been widely used for conventional polymers. In comparison, poly(3- alkylthiophenes) (P3ATs) with linear alkyl side chains, experience less steric hinderance, hence, have a rapid crystallization rate, which hinders the isothermal crystallization study from the supercooled state. Nevertheless, few attempts have been made with conventional DSC [12, 13]. In addition to the pure P3AT systems, crystallization kinetics have also been investigated for blend systems [23, 24, 25] and block copolymers [26, 27, 28, 29, 30, 31, 32, 33]. Müller et al. investigated the crystallization of P3HT-polyethylene (PE) diblock copolymer, they found that the crystal growth of P3HT block and PE block remains unaffected: onedimensional for P3HT and spherulitic growth for PE [27]. Segalman and co-workers studied the confined crystallization of P3EHT block copolymers with different flexible coil blocks such as polylactide [29], polystyrene [31], and poly(methyl acrylate) [31, 32, 33]. Lately, Coote et al. showed that the regioregularity of P3DDT is also a vital parameter for P3DDT-poly(2-vinylpyridine) (P2VP) block copolymer, by tuning the regioregularity, multiple crystallization modes become possible even at same block compositions [28].

Recently, the development of fast scanning chip calorimetry (FSC) [34, 35] enables the crystallization studies on conventional polymers with a rapid crystallization rate, such as poly (€-caprolactone) (PCL) [36], isotactic polypropylene (i-PP) [37], and branched PE [38, 39]. Luo et al. found that the crystallization rate of branched PE significantly decreases as the degree of branching increases [38]. In addition to conventional polymers, FSC has also been applied on the P3HT film deposited on gold foil and found that non-isothermal nucleation on



Figure 1: Chemical structures of poly (3-alkylthiophenes) investigated in the present work. The numbers mark the branch position, and it moves closer to the backbone from P3(4MP)T to P3(2EB)T.

cooling can be suppressed with a cooling rate of 30,000 K/s [40]. This demonstrates the capability of FSC on investigating the crystallization kinetics of CPs, which can be largely facilitated by π – π interchain interaction despite high chain rigidity. Furthermore, slow scanning at high temperatures may result in an unstable state of samples. Thus, performing fast scanning treatment to avoid chemical structural change on measurement is a must. Given that the side-chain structure plays a critical role in CPs, in the present work, we systematically investigated the side-chain structure dependence on the crystallization kinetics of five P3HT side-chain isomers: P3HT, poly (3-(4'-methylpentyl)thiophene) P3(4MP)T, poly(3-(3'-methylpentyl)thiophene) P3(3MP)T, poly(3-(2'-methylpentyl)thiophene) P3(2MP)T, and poly(3-(2'-ethylbutyl)thiophene) P3 (2EB)T, with different side-chain structures but similar molecular weights and polydispersity. Their chemical structures are shown in Fig. 1. The results suggest that the side-chain structure significantly affects crystallization kinetic for conjugated polymers. As the side chain varies from linear to branch and branch position moves closer to polymer backbone, it drastically increases steric hinderance, weakens π - π interaction and increases π - π stacking distance, resulting in more than five orders of magnitude decrease in the crystallization rate. In addition, secondary crystallization was observed for P3HT, P3(4MP)T, P3(3MP)T, and P3(2MP)T, after the rapid primary crystallization process, while P3(2EB)T only shows a slow primary crystallization behavior within experimental time window. The study shown here provides a pathway to tune the crystallization behavior of CPs through side-chain engineering. This finding can provide a new way to control the crystallization behavior for future optoelectronic materials.

Results and Discussion

Synthesis of conjugated polymers

Regioregular (r-reg) P3HT side-chain isomers (the chemical structures are shown in Fig. 1) investigated in the present work were synthesized by a quasi-living Kumada catalyst transfer polymerization (KCTP) method as reported previously [41, 42, 43, 44, 45, 46]. The polymers have a high regioregularity of

over 94%, as measured by nuclear magnetic resonance (NMR) [47]. Table 1 tabulates the molecular weight information. The polymers investigated here have similar molecular weight, polydispersity (\mathcal{D}), and regioregularity, hence, the influence of these factors to crystallization kinetics are minimized.

Thermal characterization

The temperature profile used in this study for isothermal crystallization is shown in Fig. 2. The isothermal crystallization measurements were conducted at various temperature T_a between T_g (shown subsequently) and T_m . We first heated the sample above $T_{\rm m}$ and held 10 ms to 1 s to melt all the crystals to erase its thermal history [Fig. 2(b) segments 1 and 2]. Then, we determined the needed cooling rate β to quench the sample and inhibit crystal formation [Fig. 2(b) segment 3]. Meantime, the corresponding T_g (β) can be determined. We then performed isothermal annealing at an annealing temperature (T_a) and allowed to crystallize for an extended period of time t_a (varies between 1 ms and 5.6 h) [Fig. 2(b) segment 4]. After that, the sample was quenched again to temperature below $T_{\rm g}$ to freeze the crystalline structure, followed by a final reheating scan for data analysis [Fig. 2(b) segments 5 and 6].

The thermal transitions, including $T_{\rm g}$ and $T_{\rm m}$ of P3ATs, were first characterized by conventional DSC. Among all five P3ATs, we have recently reported the thermal properties of P3HT, P3(4MP)T, and P3(3MP)T [49]. Figure 3 plots the

TABLE 1: Materials properties of P3HT isomers.

Polymer	M _n (kg/mol)	Đ	Regioregularity (%)	T _g (°C) ^a	T _m (°C)
P3HT ^b	20.0	1.05	97	16.3	224.9
P3(4MP)T ^b	20.9	1.06	97	35.9	243.8
P3(3MP)T ^b	17.3	1.68	98	41.4	260.9
P3(2MP)T	20.5	1.52	94	30.0	164.3
P3(2EB)T ^b	14.1	1.53	97	43.8	210.0

 $^{^{}a}T_{g}$ determined from DSC using the half-step method [48]. The material's property of P3HT, P3(4MP)T, and P3(3MP)T were reported in our previous work [49].

^bMolecular weight information and regularity have been published in previous works [49, 50].



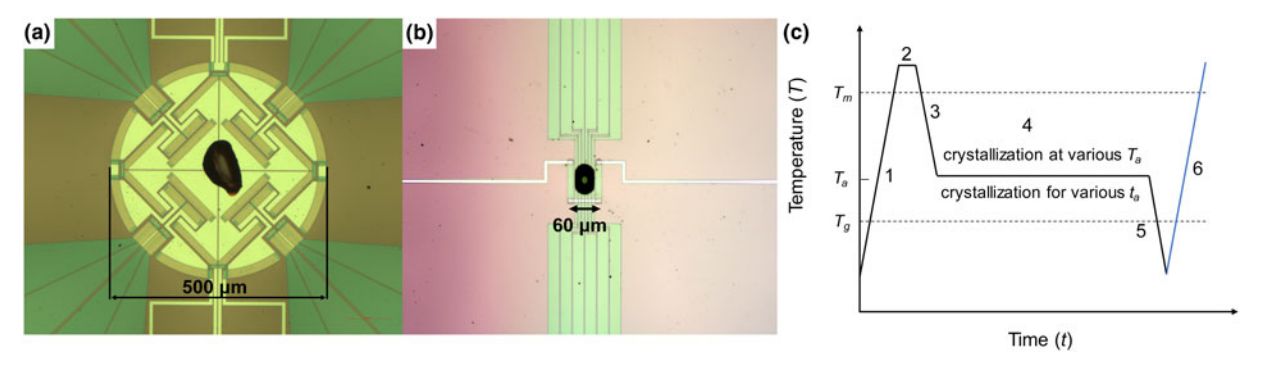


Figure 2: (a). Photograph of P3(2EB)T on a MultiSTAR UFS 1 sensor and heating area is a 500-μm diameter circle. (b) Top view of XEN-395 sensor and heating area is 60 μm \times 60 μm [51]. (c) Temperature profile of isothermal crystallization measurements for P3HT isomers. Segments 1 and 2 are removing thermal history, segment 3 is to rapidly quench the material to annealing temperature, segment 4 is isothermal crystallization with controlled temperature T_a and annealing time t_a , segment 5 is to freeze the formed crystal, and segment 6 is the heating scan for data analysis.

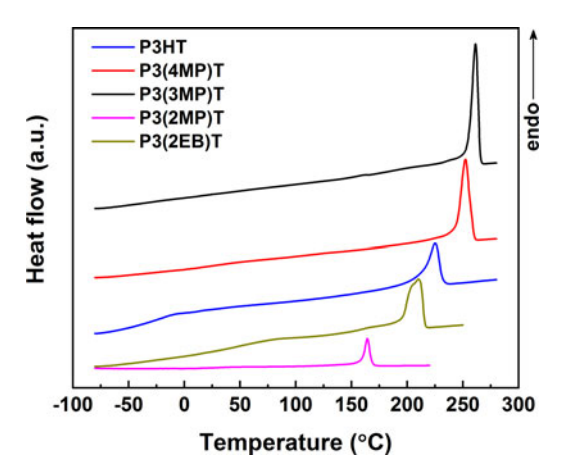


Figure 3: Determine the melt points for various P3HT isomers. Conventional DSC reheating scans of P3HT, P3(4MP)T, P3(3MP)T, P3(2MP)T, and P3(2EB)T at a heating rate of 10 °C/min.

second heating scans, and the values of $T_{\rm g}$ and $T_{\rm m}$ along with molecular weight information are tabulated in Table 1. As expected, the side-chain branch position has great influences on the thermal responses. When branch point moves closer to thiophene backbone, i.e., from P3HT to P3(3MP)T, $T_{\rm g}$ and $T_{\rm m}$ gradually increase. This trend is presumably related to the steric hindrance effect introduced by branch point as discussed in our previous work [49]. Compared to the linear alkyl side chain, branched side chain has less configuration entropy, in addition, as branch point moves closer to the backbone, it slows down the backbone dynamics and consequently, both lead to higher $T_{\rm g}$. Such steric effect argument is valid for P3 (2EB)T, which has a high $T_{\rm g}$ of 43.8 °C. Similar finding was observed in P3(EH)T by Segalman and co-workers [21]. However, it is incapable to explain a sudden decrease in T_g as branch point for methyl group further moves from position 3 to position 2. Turn to $T_{\rm m}$, a similar trend to $T_{\rm g}$ can be observed, except that P3(2EB)T being an outliner (It is worth noting here that P3(2MP)T has lowest regionegularity among the samples and has lowest $T_{\rm g}$ coincidentally. Though lower regionegularity leads to more flexible chain [52] and lower $T_{\rm g}$ [53], it is insufficient to make this conclusion based on the current data.). An investigation for the origins in future is warranted. This work will use the melting point to guide us pick the appropriate annealing temperature.

Isothermal crystallization

Given that the crystallization on cooling for the P3ATs cannot be suppressed by conventional DSC, the isothermal crystallization study was carried out with an FSC technique. FSC can quench the sample to the amorphous state with an ultrafast cooling rate of few thousands K/s. With the temperature profile scheme depicted in Fig. 2, the structure (including nuclei and crystals) formed during isothermal annealing, with the $t_{\rm a}$ ranging from 1 ms to 5.6 h (i.e., annealing time covers more than seven orders of magnitude), is frozen upon cooling below $T_{\rm g}$ and then analyzed from the subsequent reheating scan.

Figure 4 shows the reheating scans of P3(2MP)T and P3 (2EB)T at 1000 K/s after cooled down with the same rate and followed by the isothermal crystallization at 110 °C for a series of annealing time. The bulk $T_{\rm g}$ s for P3(2MP)T and P3(2EB)T at 1000 K/s cooling and heating using FSC were determined to be 42.7 and 70.6 °C, respectively. Due to a much larger cooling rate used in FSC, these $T_{\rm g}$ values are larger than those from conventional DSC [54]. For both P3(2MP)T and P3(2EB)T, only one melting peak is observed, suggesting no cold crystallization or crystal reorganization takes place on heating. As $t_{\rm a}$ increases, melting peak position slowly shifts to higher temperature, being consistent with crystal growth; in addition, with the increase of crystalline contents, glass transition broadens and $T_{\rm g}$ increases due to reduced mobility.

Since P3(4MP)T, P3(3MP)T, and P3HT crystallize much faster than P3(2MP)T and P3(2EB)T, as demonstrated in Supplementary Figs. S5–S7, measurements were carried out



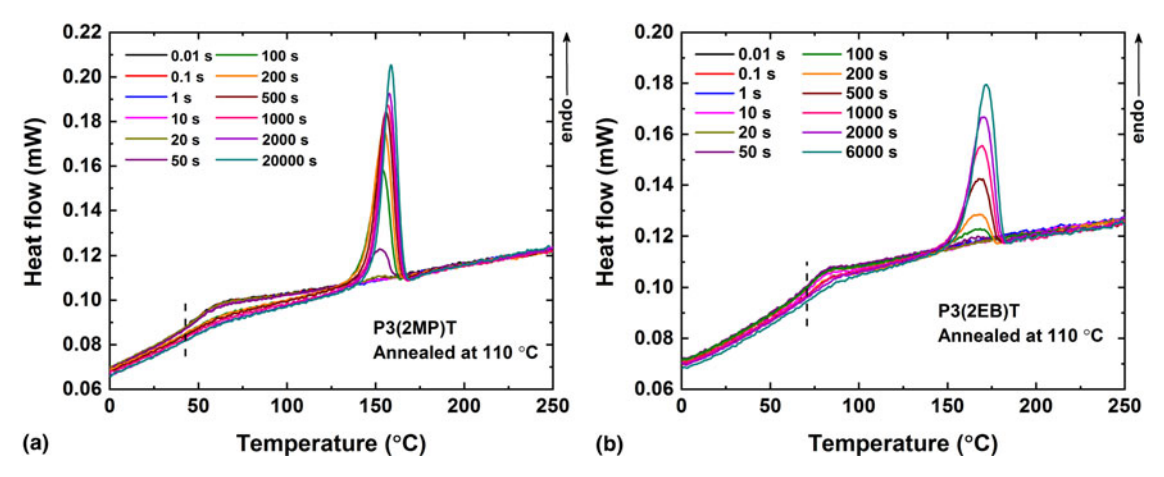


Figure 4: Reheating scans at 1000 K/s for (a) P3(2MP)T and (b) P3(2EB)T after isothermal crystallization at 110 °C for different t_a s (from 0.01 to 20,000 s, see Supplementary Figs. S3 and S4 for the reheating scans for all t_a s). The dash lines in both plots mark the bulk T_g for P3(2MP)T and P3(2EB)T at 1000 K/s cooling and heating rate.

with a much faster cooling rate of 50,000 K/s to quench the materials and the reheating scans after isothermal crystallization were performed at 10,000 K/s. Figure 5 depicts the reheating scans after isothermal crystallization at 110 °C. At short t_a s, a cold crystallization peak is observed followed by the melting peak; in addition, we notice that total enthalpy change (ΔH_{total}) (illustrated in Supplementary Fig. S8), which is the sum of the area of cold crystallization peak ($\Delta H_{\rm CC}$) and subsequent melting peak ($\Delta H_{\rm m}$), does not equal to zero (except for P3(4MP)T). These two observations suggested that there were some portion of active nuclei formed even at such high cooling rate. As t_a continues to increase, crystallites keep growing during annealing, hence, the cold crystallization peak at the subsequent heating scan decreases and a melt-reorganization process occurs, in which the less stable crystallites melt at a low temperature and recrystallize to form more stable crystallites and melt again at a higher and constant temperature.

The total specific enthalpy change in the reheating scan reflects the crystallization enthalpy during isothermal annealing, regardless the number of peaks appear. Therefore, we can obtain the isothermal crystallization kinetics by calculating ΔH_{total} , as illustrated in Supplementary Fig. S8. We performed the baseline construction based on the work by Zhuravlev and co-workers [36, 55]. First, the baseline was determined based on the number of thermal transitions on heating. In the case where only melting appears, i.e., P3(2MP)T and P3(2EB)T, the baseline was obtained by extending liquid line straight from the right to left and intersecting with the raw data; in the case when cold crystallization also presents, i.e., P3HT, P3(4MP)T, and P3(3MP)T, the baseline was obtained by connecting between the points of the onset of cold crystallization and the end of melting. Then, ΔH_{total} was calculated by integration between raw data and baseline. The data process of P3 (2MP)T and P3(2EB)T were performed with Mettler Toledo STARe software, and Origin software was used for P3HT, P3 (4MP)T, and P3(3MP)T. Figures 6(a)-6(e) depict ΔH_{total} as a function of annealing time for all five P3ATs. It is readily seen that P3(2EB)T exhibit different crystallization kinetics compared to the other four polythiophenes, i.e., P3(2MP)T, P3(3MP)T, P3(4MP)T, and P3HT show a clear linear increase of enthalpy at long t_a due to secondary crystallization in the late stage of the crystallization [36], while this is not obvious for P3

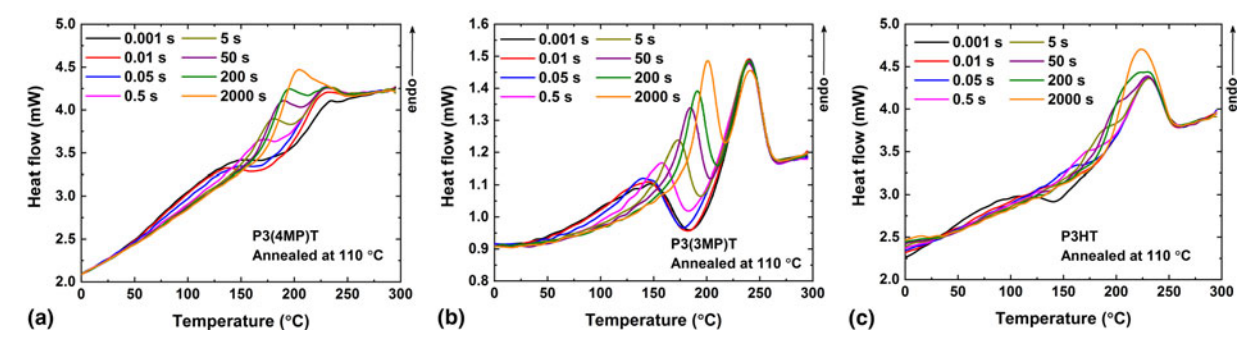


Figure 5: The reheating scans at 10,000 K/s for (a) P3(4MP)T, (b) P3(3MP)T, and (c) P3HT after isothermal crystallization at 110 °C for different annealing times (from 0.001 to 2000 s, see Supplementary Figs. S9–S11 for the reheating scans for all annealing times).



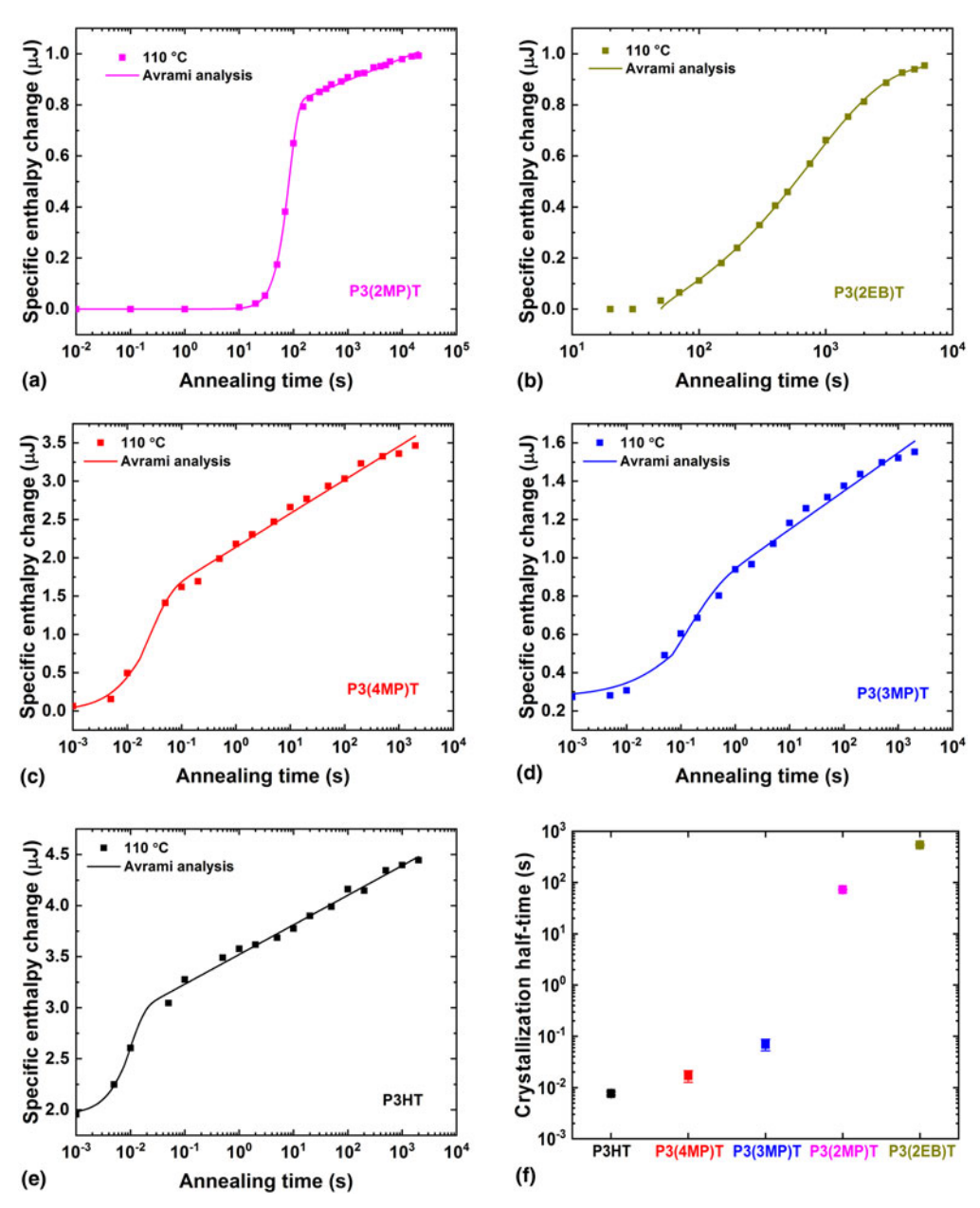


Figure 6: Specific enthalpy changes as a function of annealing time for (a) P3(2MP)T, (b) P3(2EB)T, (c) P3(4MP)T, (d) P3(3MP)T, and (e) P3HT annealed at 110 °C, respectively. The lines are the Avrami analysis curve fitting. The obtained crystallization half-time τ_c is shown in (f).

(2EB)T within the current experimental window of 5.6 h (Since, in general, secondary crystallization takes place at the later stage of the crystallization process, the lack of clear secondary crystallization in P3(2EB)T within the experimental window provides a qualitative evidence of the slowest crystallization rate). Hence, crystallization behavior for P3ATs in Figs. 4 and 5 was analyzed with two modified Avrami equations. For P3(2EB)T, we only considered a primary crystallization process with the following equation [22]:

$$\Delta H = \Delta H_{\infty} \{ 1 - \exp[-K(t - t_0)^n] \}, \tag{1}$$

where ΔH_{∞} is the final enthalpy of primary crystallization, t_0 is the induction time, K is the overall crystallization rate constant, n is Avrami index, and crystallization half-time τ_c is express as $\tau_c = (\ln 2/K)^{1/n} + t_0$. For the rest four polythiophenes, they were analyzed with consideration of secondary crystallization [36, 56, 57]:

$$\Delta H = H_{\text{int}} + \Delta H_{1,\infty} \left\{ 1 - \exp\left[-\ln 2\left(\frac{t}{\tau_c}\right)^n\right] \right\}$$

$$+ A_2(\ln t - \ln \tau_c) \times \left[\frac{1}{2}\left(\frac{|t - \tau_c|}{t - \tau_c} + 1\right)\right], \qquad (2)$$



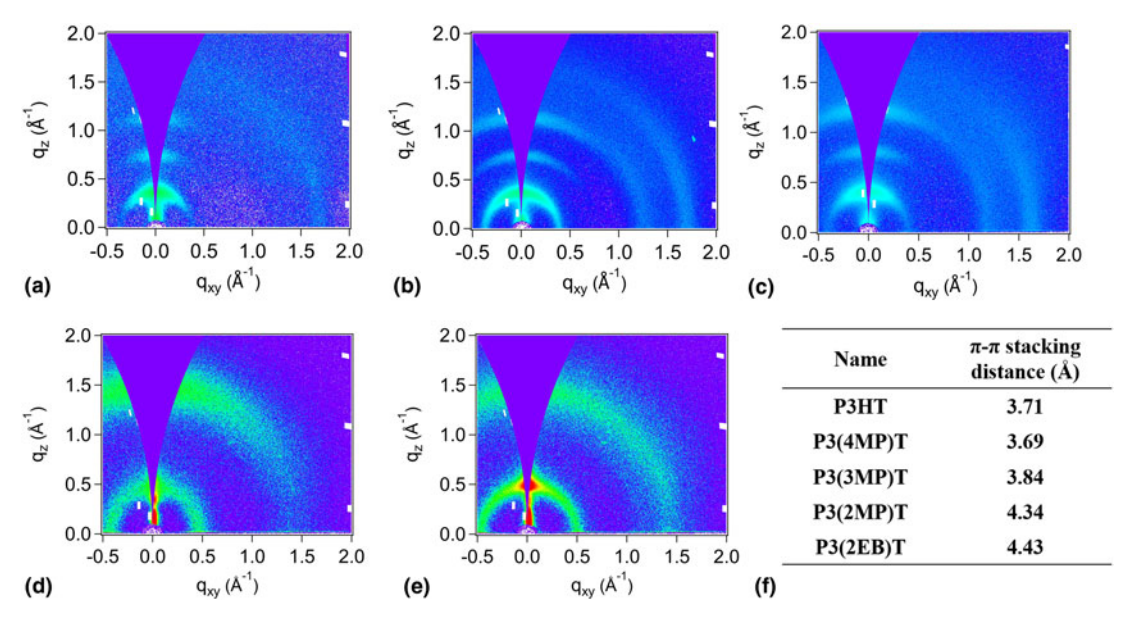


Figure 7: 2D GIWAXS profiles of as-cast (a) P3HT, (b) P3(4MP)T, (c) P3(3MP)T, (d) P3(2MP)T, and (e) P3(2EB)T. Their π-π stacking distances are tabulated in (f).

where $H_{\rm int}$ is the initial enthalpy before isothermal crystallization, $\Delta H_{1,\infty}$ is the final enthalpy of primary crystallization, and A_2 is the secondary crystallization parameter. We see that both equations well capture the evolution of crystallization with R^2 greater than 0.99, as shown in Figs. 6(a)–6(e). For P3HT and P3(3MP)T, $H_{\rm int}$ is not zero, indicating some portion of active nuclei or crystals formed during rapid cooling.

Figure 6(f) plots the model fitted τ_c for all five P3ATs. It is readily seen that the side-chain structure plays a vital role in the crystallization rate. P3HT, P3AT with linear side chain, possesses an extremely rapid crystallization rate, τ_c is approximately 8 ms. Upon introducing the branch point while still maintaining the number of carbons constant, it slows down the crystallization rate. When branch position is far away from backbone, for example, P3(4MP)T (position 4) and P3 (3MP)T (position 3), a moderate slowing down in crystallization is observed. The values of τ_c are 17 and 70 ms, respectively. By further moving branch position closer to backbone, the crystallization rate continuously reduces. The value of τ_c increases to 72 s for P3(2MP)T and 541 s for P3(2EB)T, respectively. It is worth noting here that a similar large degree of depression in the crystallization rate due to side-chain branching has been observed in polyolefins. Zhuravlev et al. investigated the crystallization of high-density PE and ethylene/1-octene copolymer, a more than three orders of magnitude decrease in the crystallization rate was observed as when 6.5 mol% 1-octene was introduced [39]. Considering that the distinct difference in backbone rigidity for PE and P3HT, yet the influence of side-chain branch on the crystallization rate is similar, suggesting a somewhat generalized phenomenon for polymers.

This depression in the crystallization rate can be related to steric effect, which affects backbone planarity and subsequently

 π - π stacking (correlated to X-ray results as discussed below). (It is worth mentioning here that for molecular OFET, π – π stacking is important for controlling the crystallization and subsequently tuning the mobility, as shown by Loo and co-workers [58, 59, 60, 61].) It has been shown that for P3HT, π – π stacking, facilitated by a strong π – π interaction between conjugated thiophene rings, is the major driving force during crystallization [62]; meanwhile, the linear side chain remains in the disordered state rather than interdigitating [11]. As the side-chain structure varies from linear to branching and branch position moves closer to backbone, steric hindrance increases. This then reduces backbone rigidity [63] and planarity, and increase π - π stacking distance, as evidenced by grazing-incidence X-ray diffraction (GIXD) results. We recently reported that π - π stacking distance increases from 3.72 Å for P3HT to 3.88 Å for P3(3MP)T [49]. Upon moving the branch position closer, for example position 2, steric hindrance further increases π - π stacking distance to 4.34 Å for P3(2MP)T and 4.43 Å for P3(2EB)T, which is among some of the highest reported π - π stacking distance, as shown in Fig. 7. Such a trend has also been reported for D-A CPs [8], such as isoindigo-based [64, 65, 66], DPP-based CPs [67, 68], and fluorene-based CPs [69]. Such a significant decrease of more than four orders of magnitude in the crystallization rate is unlike due to larger D for P3(2EB)T compared to that of P3HT and P3(4MP)T, since the D of P3(3MP)T is 1.68 and yet its crystallization rate is on a similar order as P3HT and P3(4MP)T. Subsequently, we conclude that a substantial depression in the crystallization rate for P3(2EBT) is due to the weakened π - π interaction between different planes. In addition, though close packing generally favors kinetics, in the case of alkyl stacking, we observed an opposite trend



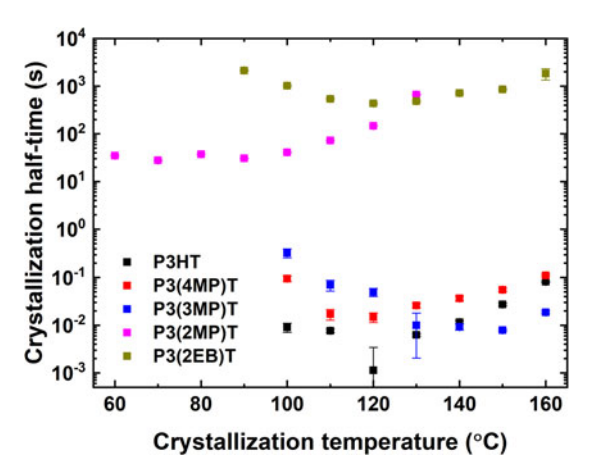


Figure 8: Isothermal crystallization half-time for P3HT, P3(4MP)T, P3(3MP)T, P3 (2MP)T, and P3(2EB)T at different crystallization temperatures.

(Supplementary Table S1): branched side chains possess closer alkyl stacking than standard P3HT yet exhibit slower kinetics. This exemplifies that the π - π interaction is the dominant contributing factor toward the crystallization rate.

We also performed the isothermal crystallization measurements on different crystallization temperatures ranging from 60 to 160 °C (see Supplementary Figs. S12-S16 for the detailed curves of specific enthalpy change as a function of annealing time) and obtained the isothermal crystallization half-time τ_c for all five P3ATs, as depicted in Fig. 8(a). A typical U-shape curve can be observed, as a result of the competition between thermodynamic driving force to promote nuclei formation and kinetic factor for nuclei growth. At low T_a (high undercooling), thermodynamic driving force (free energy difference between amorphous and crystalline phases) increases; meanwhile, kinetic factor (chain mobility) significantly decreases due to increased viscosity. On the contrary, at high T_a (low undercooling), those two competing factors show an opposite trend, i.e., thermodynamic driving force is hindered, while a kinetic factor is favorable. Therefore, it exhibits a τ_c minimum, or maximum crystallization rate, at a temperature somewhere between $T_{\rm g}$ and $T_{\rm m}$. The crystallization rate diminishes significantly as the linear side chain changes to the branch side chain and branch position moves closer to the backbone. A drastic reduction in the crystallization rate as much as approximately five orders of magnitude can be observed. It is worth to commenting here that for D-A CPs, such fine tune of side-chain structure has shown its influence on π - π stacking [8], hence, it should also affect the kinetics of long-range order (crystallites) and short-range order (aggregates), which subsequently affects the devices performance.

Conclusions

In this work, we systematically investigated the influence of the side-chain structure, specifically the branch position, on the

isothermal crystallization kinetics of five P3HT isomers: P3HT, P3(4MP)T, P3(3MP)T, P3(2MP)T, and P3(2EB)T. Conjugated polymer generally crystallizes rapidly. To suppress rapid crystallization, measurements were carried out with fast scanning calorimetry with a cooling rate up to 50,000 K/s, which permits the isothermal crystallization to be investigated in a large-temperature range. Avrami analysis was applied to analyze the isothermal crystallization kinetics. We observed a significant increase in the crystallization half-time of approximately five orders of magnitude for the primary crystallization, as side chain varies from the linear to branch structure and branch position moves closer to the backbone, for example, 8 ms for P3HT to 541 s for P3(2EB)T when isothermally annealed at 110 °C. Such a dramatic reduction in the crystallization rate has been related to the increase of steric hindrance due to the closer branch point, which increases π - π stacking distance, 3.7 Å for P3HT to 4.4 Å for P3(2EB)T, weakens π – π interaction, subsequently leads to a dramatic reduction in the crystallization rate. We also observed a secondary crystallization after rapid primary crystallization for P3HT, P3(4MP)T, P3(3MP)T, and P3(2MP)T; while P3(2EB)T exhibits a slow primary crystallization and secondary crystallization is not observed in the experimental time window we probed. In addition, a classic U-shape curve was obtained in the temperaturedependent crystallization half-time with fast crystallization locating between $T_{\rm g}$ and $T_{\rm m}$ and slow crystallization taking place when temperature close to $T_{\rm g}$ and $T_{\rm m}$. This work suggests the importance of side chain can bring into the crystallization kinetic when designing materials containing conjugated polymeric moieties.

Methodology

Grazing-incidence wide-angle X-ray scattering

Grazing-incidence wide-angle X-ray scattering (GIWAXS) was performed using a Xenocs Xeuss 2.0 SAXS/WAXS lab source instrument (Xenocs SAS, Grenoble, France). Films were directly spun cast onto a silicon wafer and exposed for 90 min in X-ray with an incident beam energy of 8.05 keV and a beam geometry of $0.8 \times 1.2 \text{ mm}$ in vacuum. The sample-to-detector distance was approximately 157 mm and the incident angle was held at 0.20 degrees. The scattering data were processed using Nika software package and WAXS tools [70].

Conventional differential scanning calorimetry

Conventional DSC measurements were carried out on a Metter-Toledo DSC 3+ (Mettler Toledo, Columbus, OH) equipped with an FRS 6+ sensor and a Huber TC 100 intracooler. Samples with 3–5 mg in mass were first heated above the melting temperature ($T_{\rm m}$) with a rate of 10 °C/min to



remove thermal history and then cooled down to -90 °C at the same rate. Reheating scans were then performed from -90 °C to $\sim T_{\rm m} + 30$ °C at 10 °C/min to determine thermal transitions including glass transition temperature ($T_{\rm g}$) and $T_{\rm m}$. Before proceeding to the isothermal crystallization measurements, cooling experiments (10-100 °C/min) were carried out on the conventional DSC and suggested that the crystallization of P3ATs cannot be suppressed with a cooling rate up to 100 °C/min, as shown in Supplementary Fig. S2 [50]. Hence, FSC technique was utilized.

Fast scanning chip calorimetry

FSC measurements were performed with a commercially available Mettler-Toledo Flash DSC 2+ and a home built ultrafast scanning calorimetry (UFDSC). For the Flash DSC 2+, with a Huber TC 100 intracooler and a MultiSTAR UFS 1 sensor, it is capable to perform measurements in the temperature range of -90 to 450 °C with scanning rates up to 10,000 K/s on heating and 4000 K/s on cooling. Dry nitrogen purge gas with a flow rate of 20 mL/min was used. Prior to measurements, UFS 1 sensor was conditioned and corrected by following manufacturer's instruction [71]. After cutting into small flakes under microscope with a scalpel, the samples were loaded onto the active heat area (a circular area of 500 µm in diameter) with an animal hair, then went through a pre-melt step to obtain good thermal contact between the sample and the sensor membrane, an example of UFS 1 sensor is shown in Fig. 2(a). Before the isothermal crystallization measurements, the samples were cooled at different rates from temperature above T_{m} to determine the desired cooling rate to quench the sample into the supercooled state. For P3(2MP)T and P3 (2EB)T, a 1000 K/s is sufficient to guench the sample to fully amorphous state as well as have a good signal-to-noise ratio, hence they were measured by Flash DSC 2+. While for P3HT, P3(4MP)T, and P3(3MP)T, they crystallize much rapidly compared to P3(2MP)T and P3(2EB)T and required much higher cooling rates to trap the samples into the glassy state, therefore, they were measured by the UFDSC and Xensor Integration XEN-395 sensor (Xensor Integration B.V., Delfgauw, The Netherlands) with a heating area (60 µm × 60 µm) was used, as shown in Fig. 2(b). To minimize the blank signal differences between reference and sample sensors, the center area of sensors was firstly cleaned by chloroform, then annealed at 453 K in vacuum for 1 h. The sample was cut into small pieces in microscale under a microscope and put directly on the heating area of a XEN-395 sensor that was calibrated using indium. UFDSC with the XEN-395 sensor allowed for well-controlled heating and cooling rates up to 50, 000 K/s between 170 and 570 K due to tiny size of the sample (<100 ng). All measurements were performed under nitrogen

at ambient pressure. The heating and cooling rate of samples measured by UFDSC are 10,000 and 50,000 K/s, respectively. Further description of UFDSC can be found in previous publications [34, 72].

Acknowledgments

This work is supported by the USM start-up grant for Z.Q., Z.C., and X.G. S.Z. also acknowledge National Science Foundation (NSF) for partial supported through office of integrative activities (OIA) by NSF OIA-1757220. L.G. thanks NSF DGE for providing support with grant NSF DGE-1449999. The instrument used in this work Flash DSC was acquired with support from ERDC. The polymers were synthesized at the Center for Nanophase Materials Sciences, which is a DOE Office of Science User Facility. S.L., T.Q., and D.Z. thank the National Natural Science Foundation of China (Nos. 21790345 and 51673094) for providing financial support. S. L. thank the Guangdong Basic and Applied Basic Research Foundation(2019A1515110647).

Author contributions

The manuscript was written through contributions of all authors. All authors have given approval to the final version of the manuscript.

Funding

This work was funded by the National Science Foundation (NSF OIA-1757220 and NSF NRT-1449999) and the National Natural Science Foundation of China (Nos. 21790345 and 51673094).

Conflict of interest

The authors declare no competing financial interest.

Supplementary material

To view supplementary material for this article, please visit https://doi.org/10.1557/jmr.2020.219.

References

- J. Mei, Y. Diao, A.L. Appleton, L. Fang, and Z. Bao: Integrated materials design of organic semiconductors for field-effect transistors. J. Am. Chem. Soc. 135, 6724 (2013).
- H. Bronstein, C.B. Nielsen, B.C. Schroeder, and I. McCulloch: The role of chemical design in the performance of organic semiconductors. *Nat. Rev. Chem.* 4, 66 (2020).



- H-R. Tseng, H. Phan, C. Luo, M. Wang, L.A. Perez, S.N. Patel, L. Ying, E.J. Kramer, T-Q. Nguyen, G.C. Bazan, and A.J. Heeger: High-mobility field-effect transistors fabricated with macroscopic aligned semiconducting polymers. *Adv. Mater.* 26, 2993 (2014).
- C. Luo, A.K.K. Kyaw, L.A. Perez, S. Patel, M. Wang, B. Grimm, G.C. Bazan, E.J. Kramer, and A.J. Heeger: General strategy for self-assembly of highly oriented nanocrystalline semiconducting polymers with high mobility. *Nano Lett.* 14, 2764 (2014).
- S. Himmelberger and A. Salleo: Engineering semiconducting polymers for efficient charge transport. MRS Commun. 5, 383 (2015).
- L. Meng, Y. Zhang, X. Wan, C. Li, X. Zhang, Y. Wang, X. Ke,
 Z. Xiao, L. Ding, R. Xia, H-L. Yip, Y. Cao, and Y. Chen: Organic and solution-processed tandem solar cells with 17.3% efficiency.
 Science 361, 1094 (2018).
- R. Noriega, J. Rivnay, K. Vandewal, F.P.V. Koch, N. Stingelin, P. Smith, M.F. Toney, and A. Salleo: A general relationship between disorder, aggregation and charge transport in conjugated polymers. *Nat. Mater.* 12, 1038 (2013).
- Y. Yang, Z. Liu, G. Zhang, X. Zhang, and D. Zhang: The effects
 of side chains on the charge mobilities and functionalities of
 semiconducting conjugated polymers beyond solubilities. *Adv. Mater.* 31, 1903104 (2019).
- J. Mei, D.H. Kim, A.L. Ayzner, M.F. Toney, and Z. Bao: Siloxane-terminated solubilizing side chains: Bringing conjugated polymer backbones closer and boosting hole mobilities in thinfilm transistors. J. Am. Chem. Soc. 133, 20130 (2011).
- F.P.V. Koch, J. Rivnay, S. Foster, C. Müller, J.M. Downing, E. Buchaca-Domingo, P. Westacott, L. Yu, M. Yuan, M. Baklar, Z. Fei, C. Luscombe, M.A. McLachlan, M. Heeney, G. Rumbles, C. Silva, A. Salleo, J. Nelson, P. Smith, and N. Stingelin: The impact of molecular weight on microstructure and charge transport in semicrystalline polymer semiconductors—poly (3-hexylthiophene), a model study. *Prog. Polym. Sci.* 38, 1978 (2013).
- R.J. Kline, D.M. DeLongchamp, D.A. Fischer, E.K. Lin,
 L.J. Richter, M.L. Chabinyc, M.F. Toney, M. Heeney, and
 I. McCulloch: Critical role of side-chain attachment density on the order and device performance of polythiophenes. *Macromolecules* 40, 7960 (2007).
- V. Causin, C. Marega, A. Marigo, L. Valentini, and J.M. Kenny: Crystallization and melting behavior of poly(3-butylthiophene), poly(3-octylthiophene), and poly(3-dodecylthiophene).
 Macromolecules 38, 409 (2005).
- S. Malik and A.K. Nandi: Crystallization mechanism of regioregular poly(3-alkyl thiophene)s. J. Polym. Sci. B Polym. Phys. 40, 2073 (2002).
- J. Balko, R.H. Lohwasser, M. Sommer, M. Thelakkat, and
 T. Thurn-Albrecht: Determination of the crystallinity of

- semicrystalline poly(3-hexylthiophene) by means of wide-angle X-ray scattering. *Macromolecules* **46**, 9642 (2013).
- C.R. Snyder, R.C. Nieuwendaal, D.M. DeLongchamp,
 C.K. Luscombe, P. Sista, and S.D. Boyd: Quantifying crystallinity in high molar mass poly(3-hexylthiophene). *Macromolecules* 47, 3942 (2014).
- 16. C.R. Snyder, J.S. Henry, and D.M. DeLongchamp: Effect of regioregularity on the semicrystalline structure of poly (3-hexylthiophene). *Macromolecules* 44, 7088 (2011).
- N.D. Treat, J.A. Nekuda Malik, O. Reid, L. Yu, C.G. Shuttle, G. Rumbles, C.J. Hawker, M.L. Chabinyc, P. Smith, and N. Stingelin: Microstructure formation in molecular and polymer semiconductors assisted by nucleation agents. *Nat. Mater.* 12, 628 (2013).
- **18. V. Ho, B.W. Boudouris, and R.A. Segalman**: Tuning polythiophene crystallization through systematic side chain functionalization. *Macromolecules* **43**, 7895 (2010).
- 19. B.W. Boudouris, V. Ho, L.H. Jimison, M.F. Toney, A. Salleo, and R.A. Segalman: Real-time observation of poly (3-alkylthiophene) crystallization and correlation with transient optoelectronic properties. *Macromolecules* 44, 6653 (2011).
- 20. D.T. Duong, V. Ho, Z. Shang, S. Mollinger, S.C.B. Mannsfeld, J. Dacuña, M.F. Toney, R. Segalman, and A. Salleo: Mechanism of crystallization and implications for charge transport in poly (3-ethylhexylthiophene) thin films. Adv. Funct. Mater. 24, 4515 (2014).
- 21. L. Yu, E. Davidson, A. Sharma, M.R. Andersson, R. Segalman, and C. Müller: Isothermal crystallization kinetics and time-temperature-transformation of the conjugated polymer: Poly (3-(2'-ethyl)hexylthiophene). Chem. Mater. 29, 5654 (2017).
- **22. M. Avrami**: Kinetics of phase change. II Transformation-time relations for random distribution of nuclei. *J. Chem. Phys.* **8**, 212 (1940).
- 23. W-R. Wu, U.S. Jeng, C-J. Su, K-H. Wei, M-S. Su, M-Y. Chiu, C-Y. Chen, W-B. Su, C-H. Su, and A-C. Su: Competition between fullerene aggregation and poly(3-hexylthiophene) crystallization upon annealing of bulk heterojunction solar cells. ACS Nano 5, 6233 (2011).
- 24. M. Da Pian, M. Maggini, G.J. Vancso, V. Causin, and E.M. Benetti: Poly(3-hexylthiophene) nanowhiskers filler in poly (ε-caprolactone) based nanoblends as potential bioactive material. Eur. Polym. J. 114, 144 (2019).
- 25. B. Risteen, M. McBride, M. Gonzalez, B. Khau, G. Zhang, and E. Reichmanis: Functionalized cellulose nanocrystal-mediated conjugated polymer aggregation. ACS Appl. Mater. Interfaces 11, 25338 (2019).
- **26.** J. Liu, E. Sheina, T. Kowalewski, and R.D. McCullough: Tuning the electrical conductivity and self-assembly of regionegular polythiophene by block copolymerization: Nanowire morphologies in



- new di- and triblock copolymers. Angew. Chem. Int. Ed. 41, 329 (2002).
- C. Müller, C.P. Radano, P. Smith, and N. Stingelin-Stutzmann: Crystalline-crystalline poly(3-hexylthiophene)-polyethylene diblock copolymers: Solidification from the melt. *Polymer* 49, 3973 (2008).
- J.P. Coote, J-S. Kim, B. Lee, J. Han, B.J. Kim, and G.E. Stein: Crystallization modes of poly(3-dodecylthiophene)-based block copolymers depend on regioregularity and morphology. *Macromolecules* 51, 9276 (2018).
- 29. V. Ho, B.W. Boudouris, B.L. McCulloch, C.G. Shuttle, M. Burkhardt, M.L. Chabinyc, and R.A. Segalman: Poly (3-alkylthiophene) diblock copolymers with ordered microstructures and continuous semiconducting pathways. *J. Am. Chem. Soc.* 133, 9270 (2011).
- 30. S.N. Patel, A.E. Javier, K.M. Beers, J.A. Pople, V. Ho, R.A. Segalman, and N.P. Balsara: Morphology and thermodynamic properties of a copolymer with an electronically conducting block: Poly(3-ethylhexylthiophene)-block-poly(ethylene oxide). Nano Lett. 12, 4901 (2012).
- E.C. Davidson, B.S. Beckingham, V. Ho, and R.A. Segalman: Confined crystallization in lamellae forming poly(3-(2'-ethyl) hexylthiophene) (P3EHT) block copolymers. *J. Polym. Sci. B Polym. Phys.* 54, 205 (2016).
- **32. E.C. Davidson and R.A. Segalman:** Confined crystallization within cylindrical P3EHT block copolymer microdomains. *Macromolecules* **50**, 6128 (2017).
- E.C. Davidson and R.A. Segalman: Thermal control of confined crystallization within P3EHT block copolymer microdomains. *Macromolecules* 50, 8097 (2017).
- **34. E. Zhuravlev and C. Schick**: Fast scanning power compensated differential scanning nano-calorimeter: 1. The device. *Thermochim. Acta* **505**, 1 (2010).
- E. Zhuravlev and C. Schick: Fast scanning power compensated differential scanning nano-calorimeter: 2. Heat capacity analysis. *Thermochim. Acta* 505, 14 (2010).
- E. Zhuravlev, J.W.P. Schmelzer, B. Wunderlich, and C. Schick: Kinetics of nucleation and crystallization in poly(ε-caprolactone) (PCL). *Polymer* 52, 1983 (2011).
- D. Mileva, R. Androsch, E. Zhuravlev, C. Schick, and
 B. Wunderlich: Homogeneous nucleation and mesophase formation in glassy isotactic polypropylene. *Polymer* 53, 277 (2012).
- 38. X. Luo, S. Xie, J. Liu, H. Hu, J. Jiang, W. Huang, H. Gao, D. Zhou, Z. Lü, and D. Yan: The relationship between the degree of branching and glass transition temperature of branched polyethylene: Experiment and simulation. *Polym. Chem.* 5, 1305 (2014).
- E. Zhuravlev, V. Madhavi, A. Lustiger, R. Androsch, and
 C. Schick: Crystallization of polyethylene at large undercooling.
 ACS Macro Lett. 5, 365 (2016).

- 40. N. Van den Brande, G. Van Assche, and B. Van Mele: Isothermal structure development in submicron P3HT layers studied by fast scanning chip calorimetry. *Polymer* 57, 39 (2015).
- N. Masuda, S. Tanba, A. Sugie, D. Monguchi, N. Koumura,
 K. Hara, and A. Mori: Stepwise construction of head-to-tail-type oligothiophenes via iterative palladium-catalyzed CH arylation and halogen exchange. *Org. Lett.* 11, 2297 (2009).
- 42. S. Tamba, K. Shono, A. Sugie, and A. Mori: C-H functionalization polycondensation of chlorothiophenes in the presence of nickel catalyst with stoichiometric or catalytically generated magnesium amide. *J. Am. Chem. Soc.* 133, 9700 (2011).
- 43. S. Tamba, S. Tanaka, Y. Okubo, H. Meguro, S. Okamoto, and A. Mori: Nickel-catalyzed dehydrobrominative polycondensation for the practical preparation of regioregular poly(3-substituted thiophene)s. Chem. Lett. 40, 398 (2011).
- 44. S. Tanaka, S. Tamba, D. Tanaka, A. Sugie, and A. Mori: Synthesis of well-defined head-to-tail-type oligothiophenes by regioselective deprotonation of 3-substituted thiophenes and nickel-catalyzed cross-coupling reaction. J. Am. Chem. Soc. 133, 16734 (2011).
- **45. R. Miyakoshi, A. Yokoyama, and T. Yokozawa**: Synthesis of poly (3-hexylthiophene) with a narrower polydispersity. *Macromol. Rapid Commun.* **25**, 1663 (2004).
- 46. M.C. Iovu, E.E. Sheina, R.R. Gil, and R.D. McCullough: Experimental evidence for the quasi-"living" nature of the Grignard metathesis method for the synthesis of regioregular poly (3-alkylthiophenes). *Macromolecules* 38, 8649 (2005).
- 47. J-S. Kim, J-H. Kim, W. Lee, H. Yu, H.J. Kim, I. Song, M. Shin, J.H. Oh, U. Jeong, T-S. Kim, and B.J. Kim: Tuning mechanical and optoelectrical properties of poly(3-hexylthiophene) through systematic regionegularity control. *Macromolecules* 48, 4339 (2015).
- 48. A. International: Standard test method for assignment of the glass transition temperatures by differential scanning calorimetry .In ASTM E1356-08. 2014. (ASTM International, West Conshohocken, PA), pp. 1.
- 49. Z. Cao, L. Galuska, Z. Qian, S. Zhang, L. Huang, N. Prine, T. Li, Y. He, K. Hong, and X. Gu: The effect of side-chain branch position on the thermal properties of poly(3-alkylthiophenes). *Polym. Chem.* 11, 517 (2020).
- 50. Z. Qian, L. Galuska, W.W. McNutt, M.U. Ocheje, Y. He, Z. Cao, S. Zhang, J. Xu, K. Hong, R.B. Goodman, S. Rondeau-Gagné, J. Mei, and X. Gu: Challenge and solution of characterizing glass transition temperature for conjugated polymers by differential scanning calorimetry. J. Polym. Sci. B Polym. Phys. 57, 1635 (2019).
- Gas Nanocalorimeters: https://xensor.nl/images/pdf-files/ Calorimeter_chips/nanogas3939.pdf.
- B. McCulloch, V. Ho, M. Hoarfrost, C. Stanley, C. Do,
 W.T. Heller, and R.A. Segalman: Polymer chain shape of poly



- (3-alkylthiophenes) in solution using small-angle neutron scattering. *Macromolecules* **46**, 1899 (2013).
- 53. S. Pankaj, E. Hempel, and M. Beiner: Side-chain dynamics and crystallization in a series of regiorandom poly(3-alkylthiophenes).
 Macromolecules 42, 716 (2009).
- Z. Qian, Z. Cao, L. Galuska, S. Zhang, J. Xu, and X. Gu: Glass transition phenomenon for conjugated polymers. *Macromol. Chem. Phys.*, 220, 1900062 (2019).
- 55. E. Zhuravlev, A. Wurm, P. Pötschke, R. Androsch, J.W.P. Schmelzer, and C. Schick: Kinetics of nucleation and crystallization of poly(ε-caprolactone) – Multiwalled carbon nanotube composites. Eur. Polym. J. 52, 1 (2014).
- 56. L. Chen, J. Jiang, L. Wei, X. Wang, G. Xue, and D. Zhou: Confined nucleation and crystallization kinetics in lamellar crystalline–amorphous diblock copolymer poly (ε-caprolactone)-b-poly(4-vinylpyridine). *Macromolecules* 48, 1804 (2015).
- 57. S. Luo, X. Kui, E. Xing, X. Wang, G. Xue, C. Schick, W. Hu, E. Zhuravlev, and D. Zhou: Interplay between free surface and solid interface nucleation on two-step crystallization of poly(ethylene terephthalate) thin films studied by fast scanning calorimetry. *Macromolecules* 51, 5209 (2018).
- S.S. Lee, C.S. Kim, E.D. Gomez, B. Purushothaman, M.F. Toney,
 C. Wang, A. Hexemer, J.E. Anthony, and Y-L. Loo: Controlling nucleation and crystallization in solution-processed organic semiconductors for thin-film transistors. *Adv. Mater.* 21, 3605 (2009).
- S.S. Lee, S.B. Tang, D-M. Smilgies, A.R. Woll, M.A. Loth, J.M. Mativetsky, J.E. Anthony, and Y-L. Loo: Guiding crystallization around bends and sharp corners. *Adv. Mater.* 24, 2692 (2012).
- 60. A.K. Hailey, A.J. Petty, II, J. Washbourne, K.J. Thorley, S.R. Parkin, J.E. Anthony, and Y-L. Loo: Understanding the crystal packing and organic thin-film transistor performance in isomeric guest-host systems. Adv. Mater. 29, 1700048 (2017).
- A.J. Petty, Q. Ai, J.C. Sorli, H.F. Haneef, G.E. Purdum,
 A. Boehm, D.B. Granger, K. Gu, C.P.L. Rubinger, S.R. Parkin,
 K.R. Graham, O.D. Jurchescu, Y-L. Loo, C. Risko, and

- **J.E. Anthony**: Computationally aided design of a high-performance organic semiconductor: The development of a universal crystal engineering core. *Chem. Sci.* **10**, 10543 (2019).
- **62. C. Melis, L. Colombo, and A. Mattoni**: Self-assembling of poly (3-hexylthiophene). *J. Phys. Chem. C* **115**, 576 (2011).
- 63. W.D. Hong, C.N. Lam, Y. Wang, Y. He, L.E. Sánchez-Díaz, C. Do, and W-R. Chen: Influence of side chain isomerism on the rigidity of poly(3-alkylthiophenes) in solutions revealed by neutron scattering. *Phys. Chem. Chem. Phys.* 21, 7745 (2019).
- 64. T. Lei, J-H. Dou, and J. Pei: Influence of alkyl chain branching positions on the hole mobilities of polymer thin-film transistors. Adv. Mater. 24, 6457 (2012).
- 65. J-H. Dou, Y-Q. Zheng, T. Lei, S-D. Zhang, Z. Wang, W-B. Zhang, J-Y. Wang, and J. Pei: Systematic investigation of side-chain branching position effect on electron carrier mobility in conjugated polymers. Adv. Funct. Mater. 24, 6270 (2014).
- 66. G.E. Park, J. Shin, D.H. Lee, M.J. Cho, and D.H. Choi: Effect of branched alkyl side chains on the performance of thin-film transistors and photovoltaic cells fabricated with isoindigo-based conjugated polymers. J. Polym. Sci. A Polym. Chem. 53, 1226 (2015).
- **67. I.** Kang, H-J. Yun, D.S. Chung, S-K. Kwon, and Y-H. Kim: Record high hole mobility in polymer semiconductors via sidechain engineering. *J. Am. Chem. Soc.* **135**, 14896 (2013).
- 68. B. Fu, J. Baltazar, A.R. Sankar, P-H. Chu, S. Zhang, D.M. Collard, and E. Reichmanis: Enhancing field-effect mobility of conjugated polymers through rational design of branched side chains. Adv. Funct. Mater. 24, 3734 (2014).
- 69. C.R. Bridges, M.J. Ford, E.M. Thomas, C. Gomez, G.C. Bazan, and R.A. Segalman: Effects of side chain branch point on self assembly, structure, and electronic properties of high mobility semiconducting polymers. *Macromolecules* 51, 8597 (2018).
- J. Ilavsky: Nika: software for two-dimensional data reduction.
 J. Appl. Crystallogr. 45, 324 (2012).
- **71. M. Toledo**: Flash DSC 2+ STAR^e System User Manual.
- **72. A.A. Minakov and C. Schick**: Ultrafast thermal processing and nanocalorimetry at heating and cooling rates up to 1 MK/s. *Rev. Sci. Instrum.* **78**, 073902 (2007).